Communications: SIF Congress 2010

K-edge radiography: Comparison of two detectors

F. Albertin

Dipartimento di Fisica dell'Università and INFN, Sezione di Ferrara - Ferrara, Italy

Summary. — Non-invasive and non-destructive diagnostics represent an important resource for historians and conservators for a deep knowledge of cultural heritage materials. K-edge radiography allows to obtain an elemental mapping of painting layers. It is performed at Larix laboratory, in Ferrara, by quasi-monochromatic X-ray beams obtained via Bragg diffraction. This technique takes advantage of the sharp rise of X-ray absorption coefficient of the elements, the K-edge discontinuity. Working at different energies, below and above the K-edge peak, allows to make the recognition of the target element. Each pigment is characterized by one or more elements; mapping an element means finding the spatial distribution of that pigment. Two different detectors have been used to perform an efficiency comparison at different energies. A commercial Front Illuminated CCD, 3075×128 pixels by Hamamatsu and an Edge-on SSD detector, designed by the Department of Science and Advanced Technology of Piemonte Orientale University, 512 Si-strip, $300 \times 100\,\mu\mathrm{m}^2$, 1 cm thick. In this paper the elemental distributions on canvas test objects with different pigment layers are presented.

PACS 78.70.Dm – X-ray absorption spectra.
PACS 07.85.Fv – X- and γ-ray sources, mirrors, gratings, and detectors.
PACS 07.05.Pj – Image processing.

1. – Introduction

The K-edge technique was originally proposed by Lehmann [1] for medical applications [2,3] and, in recent years, it has been applied in the cultural heritage field [4,5]. It takes advantage of the sharp rise of X-ray absorption coefficient of the elements, the K-edge discontinuity.

A topographic map of one pigment on the whole surface of the painting can be obtained in a reasonable time by a dual energy radiography with monochromatic X-ray beams, as produced by a synchrotron source [5]. We are investigating the K-edge technique using a portable device which consists of a quasi-monochromatic X-ray source, obtained via Bragg diffraction, of a standard X-ray beam on a mosaic crystal.
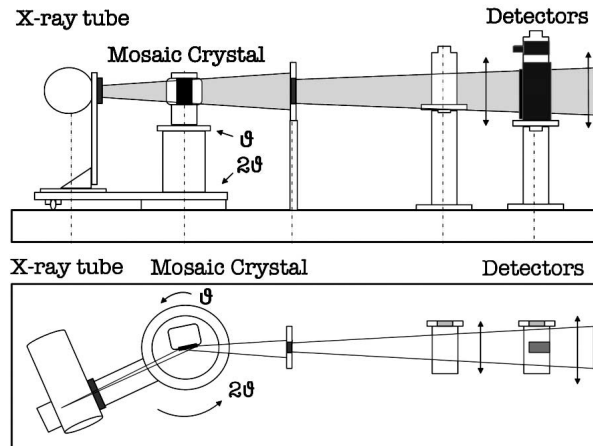

Fig. 1. – Experimental apparatus.

A defined beam energy can be set by choosing a suitable angle between source and crystal, in accordance to the Bragg law.

A mosaic crystal is formed by a large number of perfect microcrystallites which act like an aggregate of independently scattering ideal crystals with an angular distribution of the normal to the lattice planes that is roughly Gaussian [6]. As a consequence, the diffracted beam has a narrow energy band with an intrinsic energy spread related to the crystal spread ω. This type of crystal produces a quasi-monochromatic beam with a relatively high flux, necessary to perform the imaging.

Making two radiographic images with beam energies above and below the K-edge of the element under investigation, this energy choice maximizes the signal variation of target element, maintaining almost unchanged the response from the background.

The images are processed by the Lehmann algorithm to obtain two new images: the first one gives the mass density distribution (g/cm^2) of the K-edge element, while the second one gives the distribution of all other materials in the sample.

2. – K-edge facility

The K-edge radiography facility presented in fig. 1 is installed at the Larix Laboratory (Department of Physics, University of Ferrara, Italy) and provides a tuneable narrow energy band X-ray in the 7–40 keV range.

$2^.1$. *X-ray tube*. – The imaging system presented provides a tuneable narrow X-ray energy band in the 7–40 keV range by using a mammographic X-ray tube, manufactured by I.A.E (mod. XM 12, I.A.E. Spa, Milano, Italy) with a rotating molybdenum anode, a 0.5 mm beryllium window and a nominal focal spot size of $0.3\,mm^2$.

The source has been chosen to obtain a high flux by an anodic current, which can rise up to 100 mA, depending on the set-up conditions, associated to relatively low voltages, from 14 kV onwards.

High flux is required to obtain a high signal but low kVp is necessary to select, via the Bragg diffraction, only the first-order diffraction at the desired energy. For example, to perform the K-edge detection of zinc, with K-edge energy 9.65 keV, the maximum

energy of the bremsstrahlung beam must be 19.3 keV and, consequently, 19.3 kVp is the maximum high voltage to set.

For every X-ray exposition, the system allows to monitor the kVp values with an uncertainty of ± 0.1 kV and the anodic current with an uncertainty of ± 0.05 mA.

A primary collimated system, a lead slit, is placed downstream from the X-ray tube so that the dimension of the incident (and divergent) beam is approximately as the crystal size.

2˙2. *Optical table*. – The monochromator crystal is a highly oriented pyrolytic graphite (HOPG) mosaic crystal, supplied by Optigraph (Optigraph Ltd, Moscow, Russia), 60×28 mm^2 wide and 1 mm thick with a mosaic spread of $0.28°$.

The tube is mounted on an arm fixed to a motorized goniometer (Microcontrole, Evry, France) that can rotate with an accuracy of $0.001°$ to a maximum angle of $2\theta = 90°$. The crystal is placed 250 mm away from the X-ray focal spot, mounted on another isocentric goniometer that can rotate with an accuracy of $0.001°$ to a maximum angle of $\theta = 45°$.

This set-up allows to provide a monochromatic beam perpendicular to the imaging plane independently of the tuned X-ray energy.

The monochromatic beam, at a 250 mm distance from the crystal is collimated by a 8 mm width lead slit. A motorized scanning system is placed 350 mm away from the first collimator and is used as a support for the painting. A second motorized scanning system is placed 240 mm away from the first (1090 mm distance from the X-ray tube focal spot) and works as a support for the detectors. On this linear stage it is possible to place spectroscopic detectors to characterize the X-ray source or imaging detectors to realize dual energy radiography.

All the scanning systems and goniometers are connected to a multi-axis motion controller unit (MM 4006, Newport Corporation, CA, USA).

3. – Detectors

Two silicon detectors have been used to perform a comparison of element recognition of different imaging detectors: a commercial Charged Coupled Device (CCD) (S7199, Hamamatsu Photonics K.K., Japan) and a Silicon Strip Detector (SSD) realized by FBK (Foundation Bruno Kessler, Trento, Italy) on a design by the Department of Science and Advanced Technology of Piemonte Orientale University.

3˙1. *CCD*. – The Hamamatsu CCD is a FFT (Front-Illuminated) detector without FOS (Fiber Optic plate with Scintillator).

The CCD has a nominal thickness of 300 μm, a total active area of 3075×128 pixels (two different CCD chips, 1536×128 pixels) and 48 μm pixel size which allows a good spatial resolution.

The first layer of FOS, the scintillator, converts high-energy photons to visible light and fiber optics allow a high efficient photon transport to the CCD surface. This type of structure prevents the radiation damage on the silicon surface by stopping high-energy photons from reaching the bulk.

However the FOS layer presents two significant defects: on the one hand the resolution gets worse due to the non-direct detection on the silicon surface. On the other hand, low-energy X-ray photons are converted on the first layer of the scintillator surface, so that visible photons do not reach the silicon active area, making the efficiency lower.
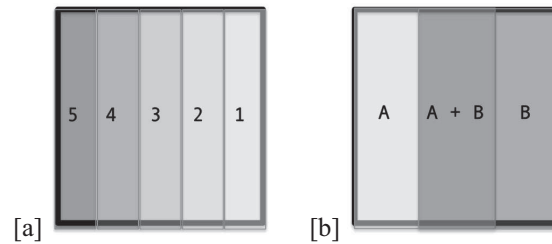
Fig. 2. – Target object structure.

To improve the efficiency at low energy and spatial resolution a CCD without FOS has been chosen.

The CCD electronics allows to set gain and offset for the two detectors independently to obtain a homogeneous signal.

3˙2. *SSD*. – The SSD has been realized with 512 Si strips, 1 cm thick and $300 \times 100\,\mu$m pixel size. It is a Edge-on detector and it works in single-photon–counting mode.

Edge-on configuration allows a major penetration thickness so to increase the efficiency in the 20–40 keV energy range. To ensure a very small dead area of the SSD working in this configuration, the detector is cut perpendicularly to the strips at a distance of only 20 μm from the end of the strips.

The SSD electronics allows to perform a calibration for each single strip to obtain a homogeneous signal along 512 strips. It is also possible to set two different energy thresholds to acquire independent signals at two different energies.

4. – Results and discussion

K-edge radiography has been performed on different test objects, realized by the *Cultural Heritage Restoration and Conservation Center "La Venaria Reale"*, in Turin, Italy. These samples have been prepared with two main aims: test the system capability to quantify the elements content in the target and identify the different superimposed layers for a list of selected pigments.

Objects with two different typologies have been realized, both on small canvas, 10×10 cm. Some of them are divided in five sections with an increasing number of layers of the same pigment, as shown in fig. 2[a]. In the second group two different pigments have been used and, in the central part of the canvas, they have been superimposed as shown in fig. 2[b].

4˙1. *Zinc*. – K-edge radiography has been applied on targets with an increasing number of superimposed pigment layers of zinc white (ZnO, Kremer Pigments, n. 46300). The painting color has been realized with a pigment proportion of 1.5 g of ZnO in 2.5 g of binder.

Since the zinc K-edge energy is 9.65 keV, radiographic images have been acquired at 9.0 and 10.3 keV. For CCD images 18 kV and 362.5 mAs have been used.

On the other hand, SSD imaging may be obtained at higher kVp because the second-order diffraction may be erased by a suitable choice of the threshold in the detector read out. For this measure 25 kV and 113 mAs have been used.

The large CCD detection area has made it possible to map the whole target. The SSD small dimensions allow only the analysis of a small fraction of the sample. The
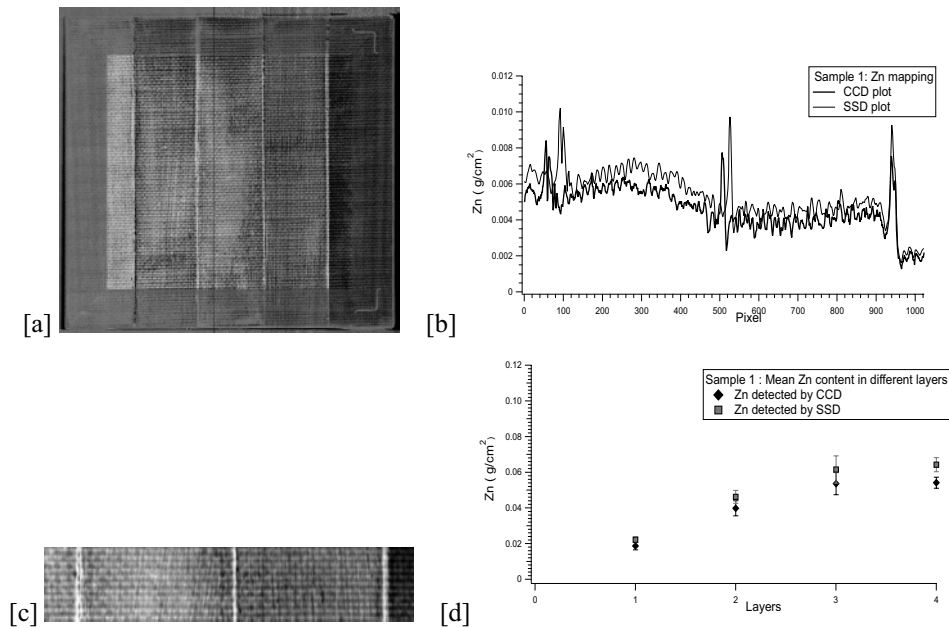
Fig. 3. – Images of zinc distribution; [a] and [c] represent Zn content (g/cm^2) detected by CCD and SSD, respectively; [b] the average zinc content by column, obtained on all SSD map and the corresponding region on CCD image; plot [d] represents the mean zinc content detected in each layer.

central part of the target has been chosen for the SSD imaging, focusing the analysis on the target side where element content is lower, *i.e.* from the single layer to the four superimposed layers.

In fig. 3[a, c] imaging results of both mappings are shown. These images represent, according to Lehmann algorithm, the element distribution in g/cm^2 on the analyzed surfaces; a higher gray level corresponds to a greater quantity of the element under study, zinc in this sample. To allow the best visual comparison, images are presented with same luminosity and contrast. It is clearly possible to identify each layer, both for CCD and SSD images.

In fig. 3[b] the average for columns of pixels of the previous images are compared. The plot in fig. 3[d] represents the zinc mean values in g/cm^2 for the four different layers obtained in CCD and SSD analysis. Error bars, which are the standard deviation of the mean zinc content of the layer, are mainly due to the canvas texture.

Plots show a fairly good compatibility between CCD and SSD measurements.

4˙2. *Arsenic*. – Since the arsenic *K*-edge energy is 11.87 keV, radiographic images have been acquired at 11.22 and 12.52 keV. For CCD images a configuration of 22 kV and 565 mAs has been used. Imaging with SSD has been performed with 25 kV and 113 mAs. The target object has an increasing number of superimposed pigment layers of Realgar (As_2S_2, Kremer pigments, n. 10800) on canvas. The painting color has been realized with a pigment proportion of 2.2 g of As_2S_2 in 2.9 g of binder. Painting layers are not homogenous and this problem is highlighted with the *K*-edge mapping, shown in fig. 4[a,c]. It is possible to identify single pigment thickening connected to little aggregates of pigment on the canvas texture. The average for columns of pixels
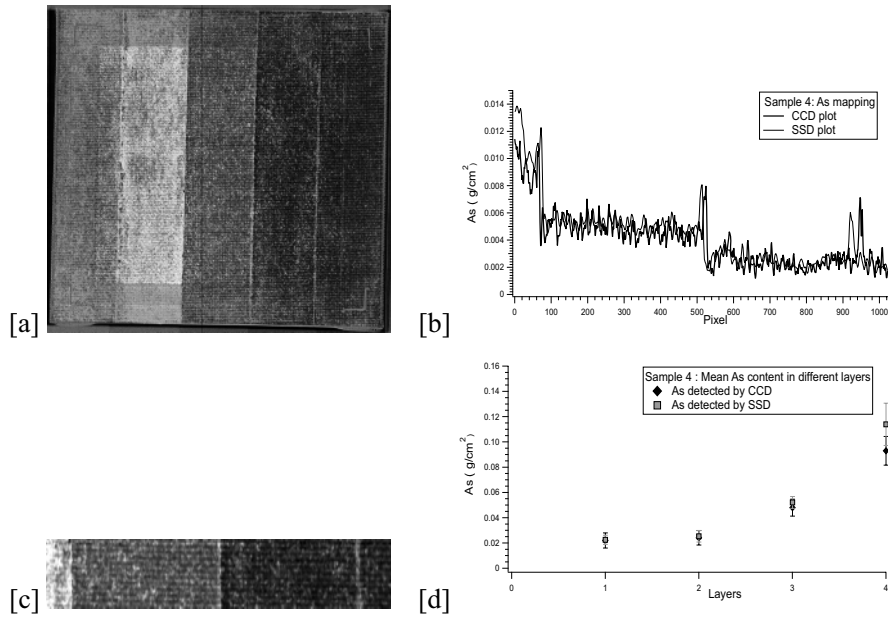
Fig. 4. – Images of arsenic distribution; [a] and [c] represents the As content (g/cm^2) detected by CCD and SSD, respectively; [b] the average arsenic content by column obtained on all SSD map and the corresponding region on CCD image; plot [d] represents the mean arsenic content detected in each layer.

in fig. 4[b] reflects the inhomogeneity in the painting layers. Furthermore, the analysis has highlighted that the arsenic content does not increase linearly with the layers number: homogenization difficulty has influenced the preparation of the test object. However, the CCD and SSD measurements have led to compatible results in terms of the arsenic content estimation.
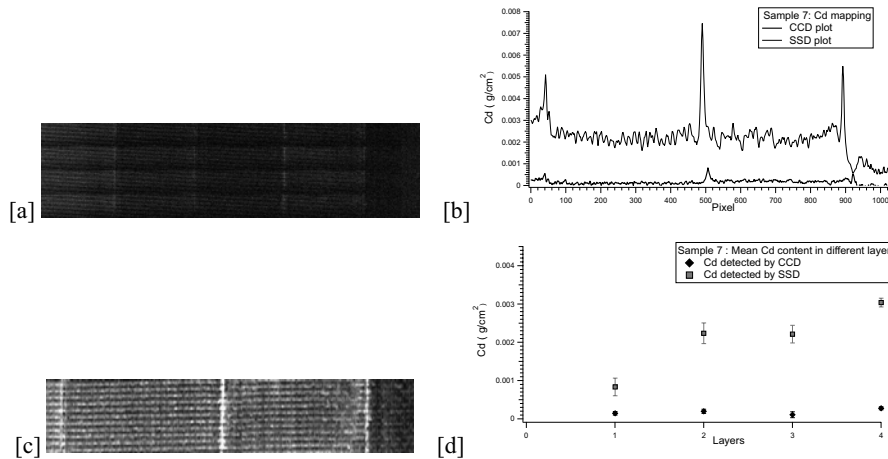

Fig. 5. – Images of cadmium distribution; [a] and [c] represents the Cd content (g/cm^2) detected by CCD and SSD, respectively; [b] the average cadmium content by column obtained on all SSD map and the corresponding region on CCD image; plot [d] represents the mean cadmium content detected in each layer.
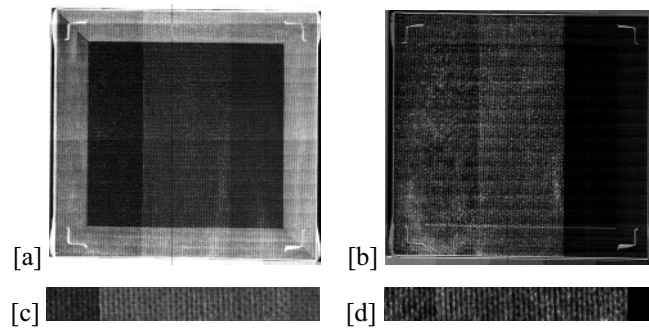
Fig. 6. – Mapping with CCD and SSD of the Zn and As distribution: the zinc compound is on the right part of the sample [a, c], and the realgar compound is on the left part [b,d].

4˙3. *Cadmium*. – The cadmium K-edge energy is 26.27 keV, therefore radiographic images have been acquired at 24.71 and 28.71 keV at maximum achievable kVp, 40 kVp. CCD images has been obtained with 431.5 mAs; with 86.3 mAs for SSD. Target objects with an increasing number of superimposed pigment layers of cadmium red (CdS + CdSe, Kremer pigments n. 21140) have been analyzed. The painting color has been realized with a pigment proportion of 2.1 g of powder in 2.4 g of binder. A comparison between
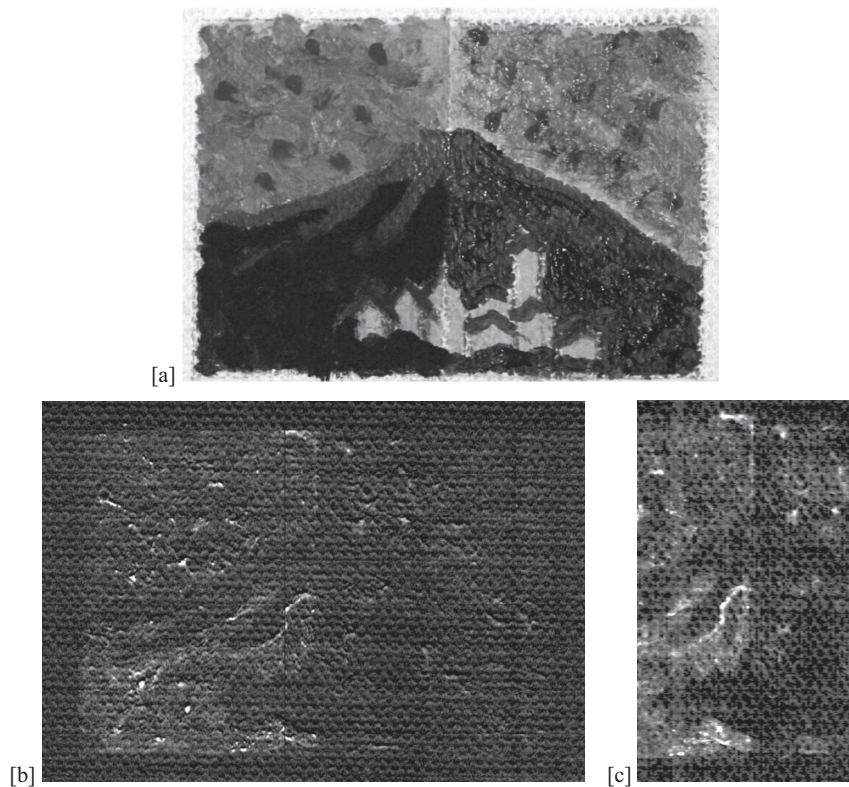

Fig. 7. – Zinc mapping of the painting [a] with CCD [b] and SSD [c] detectors.
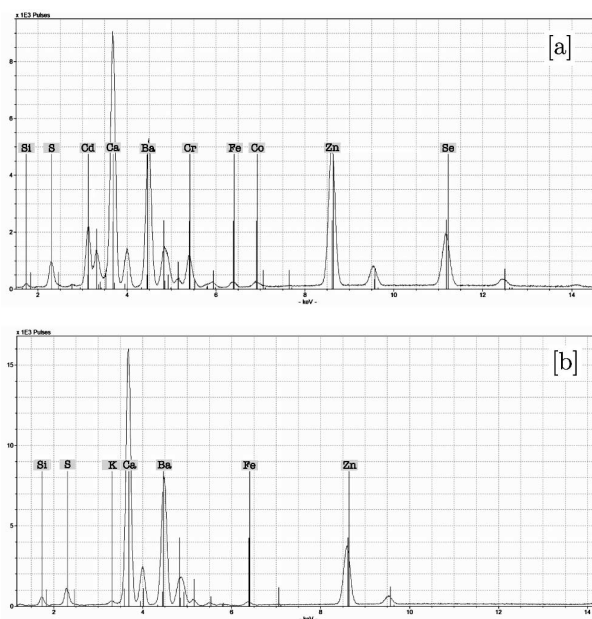
Fig. 8. – XRF analysis on the test painting: [a] analysis results on painting layers, [b] analysis on canvas where zinc presence is highlighted.

the K-edge mapping realized with CCD and SSD is shown in fig. 5[a,c]. Due to the low efficiency of the front-illuminated CCD detector at this energies, a very small amount of cadmium is detected by CCD (fig. 5[d]).

4˙4. *More complex sample*. – A second target type, where cadmium yellow (CdS + ZnS, Kremer pigments n. 21020) and realgar (As_2S_2, Kremer pigments n. 10800) have been superimposed in the central part, has been analyzed. A K-edge radiography on two different elements, zinc and arsenic, has been performed. The zinc and arsenic distributions, obtained with energies, kVp and current condition as in **4**˙1 and **4**˙2, are shown in fig. 6[a,b]. The element distribution images show a good separation between the two pigments.

5. – Test painting

A test painting has been realized using on the left hand zinc, cadmium, chromium and cobalt pigments and, on the other side, organic pigments. In fig. 7 the CCD and SSD zinc mapping is shown. A higher Zn content is detected in the left part of the painting. Unexpected zinc has been detected in the right part where only organic pigments have been used.

This was explained by the XRF analysis, which highlighted Zn, Cd, Cr and Co content in the left side (fig. 8[a]) but also a zinc content used for the canvas preparation on the right part of the painting (fig. 8[b]).

6. – Conclusions

K-edge technique has been successfully tested in the detection of zinc, arsenic and cadmium pigments. Elements have been imaged and mapped in different situations.

A good quantitative correspondence between CCD and SSD has been found. SSD presents a higher efficiency at energies above 20 keV, CCD detector allows faster acquisition due to the large detection area.

Work is in progress to study the capability of the system to perform quantification of the mass density on different pigments and applications on paintings *in situ*.

REFERENCES

[1] LEHMANN L. A., ALVAREZ R. E., MACOVSKI A. and BRODY W. R., *Med. Phys.*, **8** (1981) 659.
[2] LEWIS R., *Phys. Med. Biol.*, **42** (1997) 1213.
[3] BALDELLI P., TAIBI A., TUFFANELLI A., GILARDONI M. C. and GAMBACCINI M., *Phys. Med. Biol.*, **50** (2005) 2225.
[4] BALDELLI P., BONIZZONI L., GAMBACCINI M., GARGANO M., LUDWIG N., MILAZZO M., PASETTI L., PETRUCCI F., PRINO F., RAMELLO L. and SCOTTI M., *Nuovo Cimento*, **29** (2006) 663.
[5] KRUG K., DIK J., DEN LEEUW M., WHITSON A., TORTORA J., COAN P., NEMOZ C. and BRAVIN A., *Appl. Phys. A*, **83** (2006) 247.
[6] OHLER M., SANCHEZ DEL RIO M., TUFFANELLI A., GAMBACCINI M., TAIBI A., FANTINI A. and PARESCHI G. J., *Appl. Cryst.*, **33** (2000) 1023.